



# Manipulated Magnetic Nano Particles for Photonic Biomedical Mapping

Adi Vegerhof, Arkady Rudinzky, Yevgeny Beiderman, Hamootal Duadi,  
Rachela Popovtzer, and Zeev Zalevsky\*

*Faculty of Engineering and Institute of Nanotechnology and Advanced Materials, Bar-Ilan University, Ramat-Gan, 52900, Israel*

Our main goal is to develop a new speckle based imaging modality for biological applications. The method is based on detection and manipulation of targeted conjugated magnetic nanoparticles (MNPs), which can specifically target cells or other live tissue, and form a concentrated assembly yielding speckle imaging capabilities. The MNPs detection technique employs temporal tracking of secondary speckle patterns while applying a magnetic excitation field that oscillates the particles. We experimentally demonstrate that placing MNPs in an alternating current (AC) electromagnetic field gives rise to modulation of incident light scattered from the material. It was found, via *in vitro* and two *ex vivo* experiments, that the resultant modulation spectrum of the speckle patterns is directly associated with the chemical properties such as different sizes, concentration and chemical coating of the MNPs. In *ex vivo* experiment we demonstrate the potential of the proposed speckle imaging method for detecting the presence of arterial plaque. By taking those results into consideration, the method holds a great promise for non-invasive speckle imaging.

**Keywords:** Magnetic Nanoparticles (MNPs), Speckle, Atherosclerosis, Molecular Imaging, Speckle, Magnetic AC Field.

The most common noninvasive whole body imaging techniques to diagnose the existence of damaged or distorted tissues used nowadays are computed tomography (CT) and magnetic resonance imaging (MRI). CT is a costly and relatively high-dose procedure, with high levels of radiation leading to increase the probability of cancer.<sup>1–3</sup> Both CT and MRI methods are often combined with an injected contrast medium to improve the visibility of internal body structures. Despite the many advantages of these methods, MRI is associated with long image acquisition time, high costs and high processing noise because it requires a significant electric current supply with relatively low sensitivity, the CT is associated with high ionizing radiation.<sup>4,5</sup> Therefore, the development of a simple and accurate detection method which will overcome these limitations is highly desirable. Optical techniques are possible alternatives; however they suffer from two basic drawbacks. First of all, the optical penetration depth limits the use of optical techniques to subcutaneous applications. Second, the contrast between different physiological states is very low and only by adding contrast agents the later can be solved, and drug delivery is possible.

The main goal of this work is to develop a simple and highly sensitive optical detection technique in which bio-functionalized magnetic nano particles (MNPs) are intravenously administered and specifically directed, by an external magnetic field, to specific cells and tissue. By using magnetic contrast agents we allow the integration of diagnostics and therapy, as well as guiding the particles to a specific area via magnetic field. The MNPs primary quality is their reaction to external magnetic field; this feature has been utilized in applications such as drug targeting and bio separation including cell sorting. Today the use of tissue speckle imaging is specially focused on monitoring tissue thermal modification, monitoring tissue velocity and circulation, imaging techniques observing tissue deformation and tissue motion.

By applying laser illumination MNPs change the typical speckle fingerprint of targeted tissue, which is different from that of non-targeted tissue. In the present work we show a proof of concept, both *in vitro* and *ex vivo*, in which analysis of the temporal changes of the scattered secondary speckle patterns denotes the existence of MNPs. In addition, various MNP dimensions and biochemical coatings have diverse temporal motion characteristics which can assist in differentiating between various tissue characteristics.<sup>6–8</sup> Surface modifications of MNPs

\*Author to whom correspondence should be addressed.

expand their utilization by enabling them to target specific sites on cell surfaces.<sup>9</sup> MNPs act as super-paramagnetic materials in the sense that their magnetism depends upon the existence of an external magnetic field and prevents their aggregation.<sup>10–13</sup> In this article we used Chemicell, magnetite core MNPs, classified as super-paramagnetic nanoparticles.<sup>12</sup>

Our detection technique is based on temporal analysis of time varying secondary speckle patterns. Those patterns obtained when the illuminating laser light is back scattered from the MNPs movement in the inspected sample.<sup>14–19</sup>

When the speckle pattern changes in time, due to changes in the properties of the scattering/back reflecting medium in biological materials, this phenomenon is also known as bio-speckle.<sup>17, 20, 21</sup> We use laser illumination that interacts with the MNPs and cause scattering that results in secondary speckle patterns. Then we analyze the temporal changes of the secondary self-interference speckle patterns obtained due to the coherence of our light source. The slightest changes in phase affects the intensification of the self-interference patterns and allows us to extract visualize the displacement of the manipulated nanoparticles.

The work presented in this paper combines an optical system to capture MNP movement and electrical system to produce the magnetic field that controls motion of MNPs. For this purpose, an MNP sample was placed on top of a coil producing an alternating magnetic field (AC). Simultaneously with the AC magnetic field, the MNP sample was illuminated by a monochromatic green laser beam ( $\lambda = 532$  nm) and the scattered light was recorded by a conventional charged coupled (CCD) camera. The video sequence was analyzed to evaluate the amplitude of the displacement spectrum.

The optical system includes an inverted microscope (BX51, Olympus) (Fig. 1(a)). The object was illuminated with a green DPSS laser at a wavelength of 532 nm (DPGL-2100, Photop suwtech). The laser was set on an oblique angle of  $\sim 450$  towards the sample (Fig. 1(b)) with an output optical power of 30 mW. The oblique angle was chosen to be higher than that defined by the NA of the objective lens. This was done to avoid collecting transmitted illumination directly. The speckle pattern was imaged using a CCD camera (PL-A741-E, PixeLink) with pixel size of  $6.7 \mu\text{m} \times 6.7 \mu\text{m}$ . The imaging lens was properly defocused to allow translation of the angular tilt movement into lateral movement of the random speckle pattern.<sup>19</sup>

The electrical system includes an electro-magnet made of copper coil surrounding an EC Ferrite core, with  $30 \Omega$  resistance, connected to a waveform generator that sets the voltage and frequencies provided to the coil. A  $10 \Omega$  resistor is connected to the coil.

Tracking the lateral movement is a simple numerical task that can be realized using a basic correlation based algorithm. The relative shift of the correlation peak from the first frame is linear, and proportional to the actual movement of the MNPs. The dependency of the value of

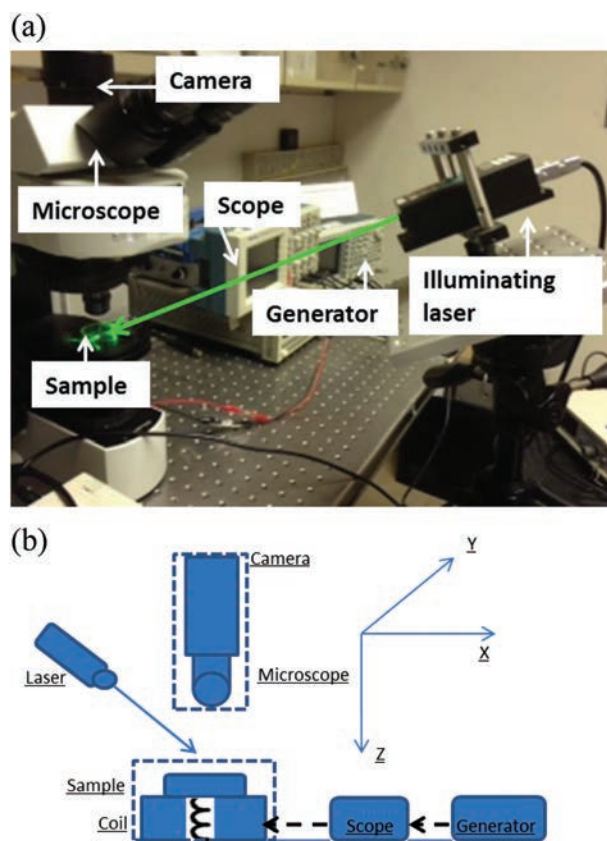


**Fig. 1.** Description of experimental setup. (a) Image of the experimental setup. (b) Scheme of the electrical circuit which induces the magnetic field.

the correlation function on the axial position is modeled (for continuous functions  $f$  and  $g$ ) with the assumption of uniform intensity at the object plane (being the diffusive source that generates the secondary speckle distribution). The correlation function of the intensity between two functions is defined as:

$$(f * g)[n] \stackrel{\text{def}}{=} \sum_{m=-\infty}^{\infty} f^*[m]g[n+m] \quad (1)$$

Where  $f^*$  denotes the complex conjugate of  $f$ .

Thus, the 2-D movement estimation includes computation of the correlation peak for the captured time moving speckle patterns, while from the time varying peak position we extracted the information regarding angular tilting movement of the back reflecting surface. From the value of the correlation we might obtain the information of the axial movement, as such movement might be related to the change in spatial distribution of the speckle pattern.<sup>14, 16, 18, 20, 22, 23</sup>

The flow chart of the algorithm, represented in Figure 2, is used for analyzing MNP movement. Analysis was done using Matlab. The camera captures a video sequence with 27 fps, while Matlab software tracks the movement of the reflected/scattered speckle patterns and extracts the 2-D tilting change in time.

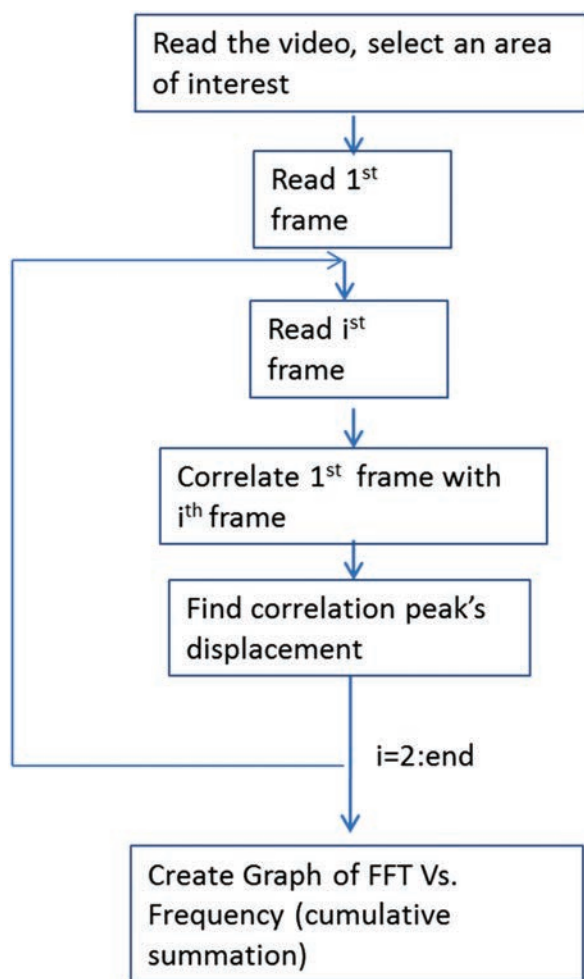


**Fig. 2.** Flow chart of the computation algorithm.

The MNPs we use have a magnetite core, as imaged by transmission electron microscopy (TEM) in Figure 3(a). Those MNPs are produced by Chemicell and have different chemical parameters such as coating, size and concentration. We used three coating types: Amine (functional group: Amine—NH<sub>2</sub>), Oleic Acid (functional group: Sodium carboxylate, COO—Na<sup>+</sup>), and Dextran (functional group: Hydroxyl groups) that can create ionic bonds, as schemed in Figure 3(b). Although different types of coatings were used, the total hydrodynamic diameter (twice the thickness of the coating and the diameter of the iron oxide core) of the coated MNPs was 200 nm. These coating types have different functional groups that can create a covalent coupling of biomolecules (antibodies or proteins) used as linkers for conjugation with antibodies to reach targeted cells.

In this proof of concept experiments we used MNPs that have a combination of properties required for a safe and efficacious strong magnetic responsiveness in the absence of magnetic memory. The MNPs are also made from fully biocompatible components and their size was matched to the type of interaction we aimed to measure. The utility

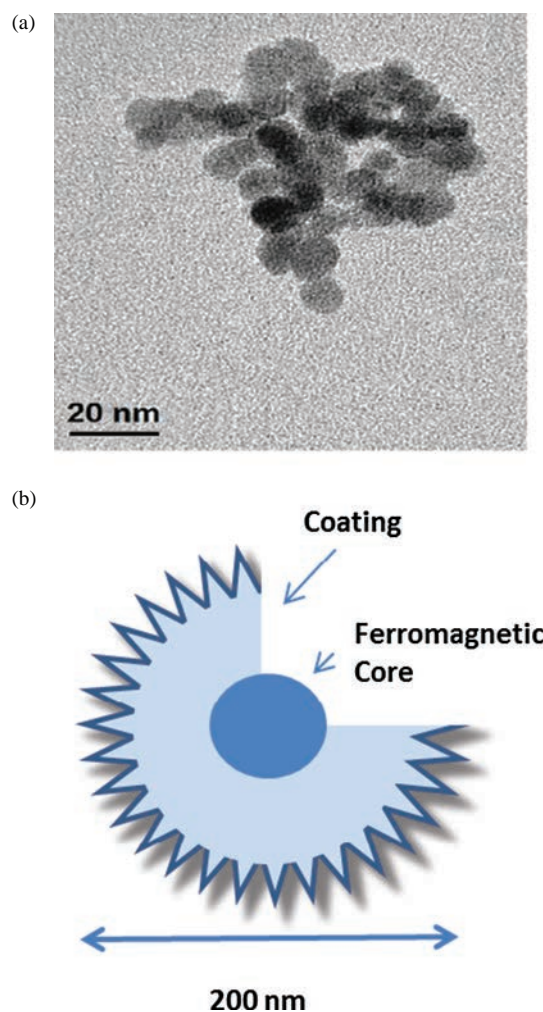


**Fig. 3.** (a) TEM image of ferromagnetic core, (b) Scheme of 200 nm magnetic particle with coating.

of the algorithm in estimating horizontal displacement of 200 nm Amine coated MNPs in aqueous solution at 10 mg/ml concentration under magnetic field, is presented.

In order to analyze the feasibility of speckle imaging using MNPs, we placed an aqueous solution (distilled ionized water) as the sample and applied an external magnetic field by applying 4 V and 3 Hz to our coil based excitation circuit. Then, we added MNPs to the aqueous solution sample and examined the changes in the speckle pattern. As seen in Figure 4, the aqueous solution (green line) has a very low reaction to the excitation frequency at 3 Hz, while the sample containing MNPs (blue line) shows a significant peak at 3.1 Hz.

To examine the relationship between the excitation frequencies and MNP displacement, we used MNPs under magnetic fields by applying 4 V input. There is high correlation between MNP displacement peaks (1.35, 1.9 and 3.38 Hz) measured by our speckle detection technique and excitation frequencies (1, 2 and 3 Hz) ( $r = 0.96$ ,  $p < 0.001$ ), as shown in Figure 5(a). In this figure, in order

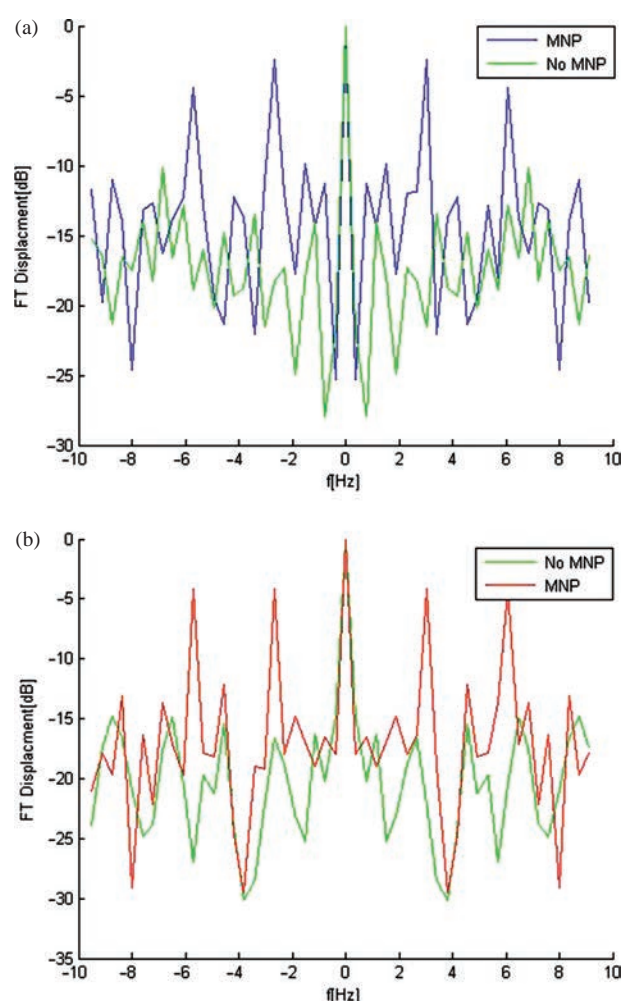


**Fig. 4.** Comparison of displacement spectrum with and without MNP. Displacement spectrum of the 200 nm MNPs, at concentration of 10 mg/ml, 4 volt and 3 Hz (blue), and deionized water without MNPs (green).

to focus the graph on the first introduced peak (marked), we eliminated the repeatable peaks. The accuracy of the optical configuration in tracking particle displacement includes tracking movement not only in transverse plane but displacement due to tilt and axial related shift as well. When looking at the statistical distribution of 30 experiments (Fig. 5(b)), one may notice that change in magnetic field frequency alters the frequency of the temporal displacement peak, while maintaining its average amplitude.

By increasing the voltage, the magnetic field is increased.<sup>26</sup> Hence in higher voltage we see stronger speckle displacement (Fig. 5(c)). For example, with 4 V a 10% higher peak is obtained than with 2 V, while the frequency of the temporal displacement peak remains the same. The statistical distribution of 30 experiments (Fig. 5(d)), indicates that change in magnetic field voltage alters the average amplitude of the temporal displacement peak while maintaining its movement frequency.

To understand the influence of different chemical parameters on displacement, we first examined MNPs with various coatings (Dextran, Oleic acid and Amine, as mentioned above). The magnetic field was obtained by applying 4 V and an excitation frequency of 2 Hz. Figure 6(a) shows that the apparent peaks for MNPs with Dextran are shifted by 16% to the left compared to the peaks obtained with Oleic acid and Amine (1.14 and 0.96 respectively). In Figure 6(b) we can see that Oleic acid and Amine coatings mainly alter the frequency of the temporal displacement peak, while Dextran changes the average displacement amplitude as well.

We compared the displacement of 50 nm, 100 nm and 200 nm MNPs under magnetic field (green, red and blue lines respectively in Fig. 6(c)). In Figure 6(d) one can see that the increase in MNP diameter decreases the frequency of the temporal displacement peak, while at the same time, increasing the displacement amplitude.<sup>27</sup> For example the two peaks obtained for 200 nm and 100 nm MNPs are differentiated by 30% in amplitude (−2.8 and −4.0 respectively) and have a temporal frequency shift of 6%, while 200 nm and 50 nm MNPs are differentiated by 60% (−2.8 and −6.8 respectively) and have a temporal frequency shift of 30%. This indicates the possibility of distinguishing between particle sizes *in vivo*, by using the proposed secondary speckle analysis approach.

Changes in particle concentration lead to changes in the speckle intensities. However this has no relevance to displacement, but rather to the accuracy of measurement. We compared the speckle pattern obtained with different concentrations: 5 and 10 mg/ml solutions (red line and blue line respectively in Fig. 6(e)). As seen in Figure 6(f), even though the solution was diluted by 50%, the amplitude of the displacement peak measured in the 5 mg/ml solution was lower by only 9.5% than the peak in the 10 mg/ml solution. Furthermore, the frequency of the temporal displacement peak remained the same.

The chemical parameters affect the generated displacement map, the MNPs different coating changes the type and the strength of the chemical connections to the related lesion and the aggregation size thus influences the particle moments in the axial dimension.<sup>23,27</sup> The different size of MNPs changes the distance between the wall and the MNPs and between the magnetite cores, thus changes the local gradient magnetic field on the MNPs.<sup>28</sup> MNPs concentration changes the number of captured MNPs along the axial direction, resulting in the decrease of the particles concentration and distribution along the vessel. All of the electrical and chemical parameters that have been tested are summarized in Table I.

An important parameter concerns the buffered solution of the MNPs for which the optical phenomenon arises. The mapping of the MNPs displacement with different MNP solvent would constitute clear results that the displacement is a direct result of the MNPs movement only. A phosphate

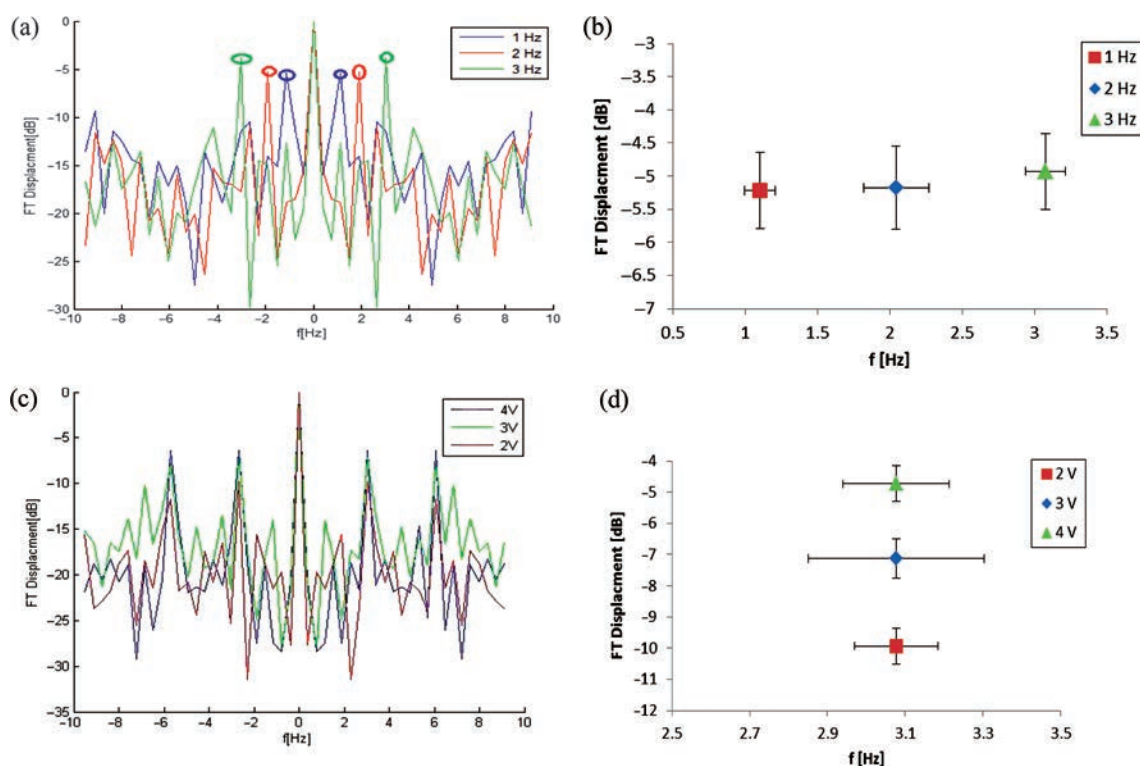


**Fig. 5.** Influence of electrical parameters (frequency and voltage) on the displacement spectrum. (a) Displacement spectrum and (b) average amplitude of displacement spectral peak of 200 nm MNPs, at a concentration of 10 mg/ml, 4 volt and 1 Hz (blue), 2 Hz (red) and 3 Hz (green). (c) Displacement spectrum and (d) average amplitude of displacement spectral peak of 200 nm MNPs, at concentration of 10 mg/ml at 3 Hz and 4 V (blue), 3 V (red) and 2 V (green).

saline buffer was used to ensure that the salt strength will not affect the results. As seen in Figure 6(g), the phosphate buffer and DI water exhibit the same pattern of results with no significant change between the two peaks' heights that leads to the unequivocal conclusion that the displacement received is the MNPs movement only.

Chicken skin was used to examine the influence of tissue on the performance of the proposed optical measurement system. The magnetic field was obtained by applying 4 V and excitation frequency of 3 Hz. Figure 7(a) shows the apparent peaks at 3.04 Hz in the blue line and 3.4 Hz in the red line. These peaks compared to the apparent peaks at Figure 5(a) are shifted due to the scattering and absorption characteristic of the tissue itself. The peaks obtained show 8.5% stronger displacement and 9% lower temporal frequency compared to the peaks obtained without tissue screening (Fig. 7(b)). Both these differences can be explained by the blurring effect of the tissue: it broadens the temporal and axial dimensions (displacement) hence decreasing temporal frequency.

In the upper panels of Figure 8, we see the middle cross sections of a coronary artery, while the lower panels show the same slices after MNP conjugation. It seems that the particles are moving and making the image blurry and unclear. The scan indicates that the particles aggregate on the plaque. After scanning the artery, we slice it lengthwise

so the cross section holds the maximal amount of plaque and MNPs.

As we can see, no significant pattern is obtained without the particles (red in Fig. 9(a)) no particle corresponds to the magnetic field. As expected, the MNPs conjugated to the plaque respond to the magnetic field (blue line in Fig. 9(a)). A magnetic field of 4 V was applied and the frequency changed from 1 to 3 Hz, as seen in Figure 9(b). The same temporal frequencies as shown in Figure 9(c) are seen in Figure 5(a), with weaker ( $\sim 30\%$ ) peak values, due to MNP attachment to the plaque surface, restricting their movement. Figure 9(d) exhibits the displacement pattern of 3 Hz while applying voltages of 2, 3 and 4 V in the magnetic field generation circuit. This figure is comparable with Figure 5(c) pattern but has weaker peak's values ( $\sim 26\%$ ). The temporal behavior of the MNPs exhibited in Figure 9(e) is the same as seen in Figure 5(d). Those results show that the attached particles have identical behavior as the non-attached particles. This result strengthens our vision of highly accurate imaging technique for specific tissues. Note that the difference between Figure 9(a) and Figure 4 is that in Figure 9(a) a speckle pattern is taken from the artery while in Figure 4 we show the speckle pattern of particles on a sample plate in aqueous solution.

The frequency of displacement depends on the mechanical properties of the nanoparticles and their environment.

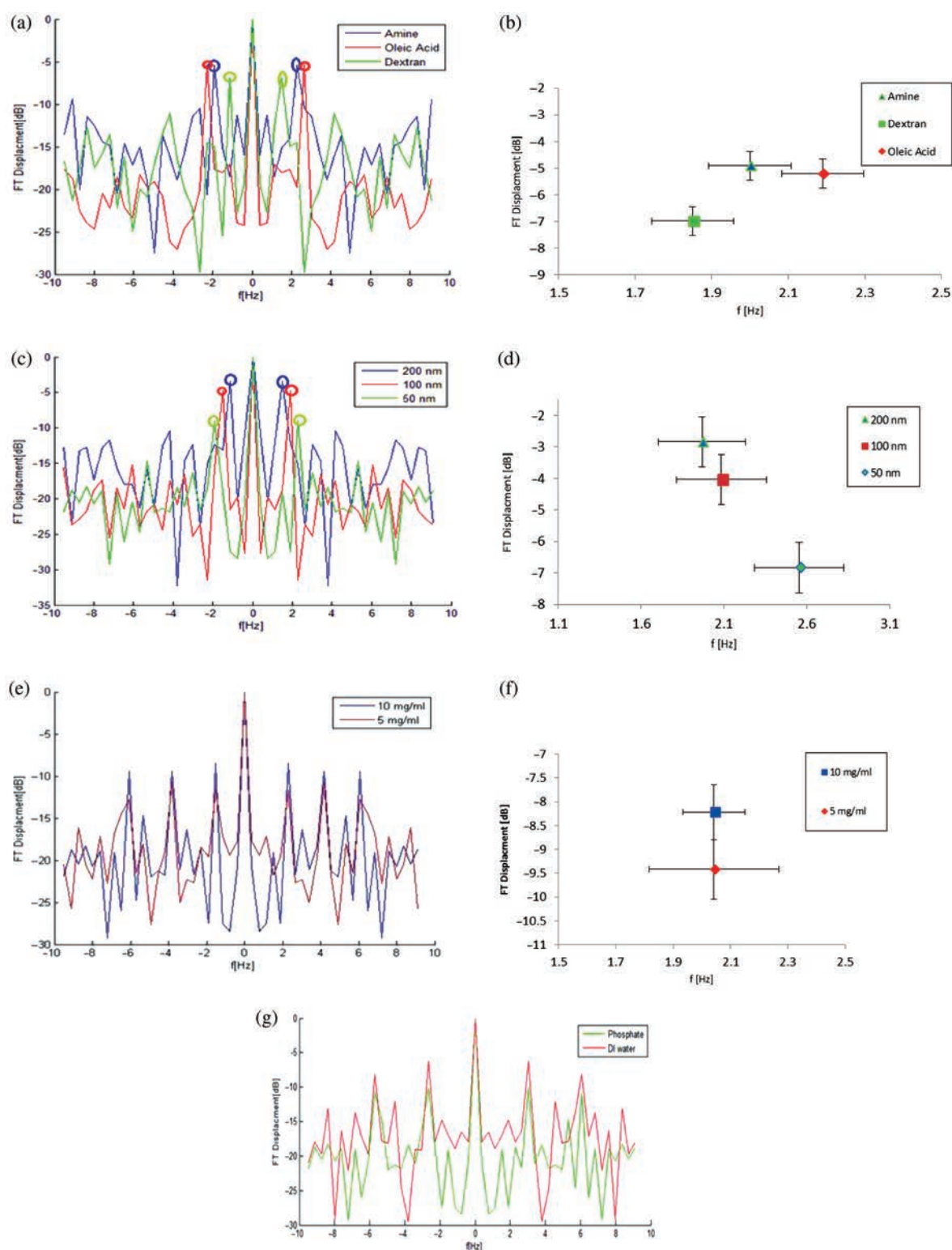


**Fig. 6.** Influence of MNP's chemical parameters (coating, size, concentration and buffered solution) on the displacement spectrum. (a) Displacement spectrum and (b) average amplitude of displacement spectral peak of MNPs, at concentration of 10 mg/ml at 2 volt and 1 Hz with different coatings: Dextran (blue), Oleic acid (red) and Amine (green). (c) Displacement spectrum and (d) average amplitude of displacement spectral peak of MNPs, at concentration of 10 mg/ml at 2 volt and 1 Hz with different Amine coated MNPs sizes: 200 (blue), 100 (red) and 50 (green) nm (e) Displacement spectrum, (f) average amplitude of displacement spectral peak of MNPs, at 4 volt and 2 Hz at concentration of 10 mg/ml (blue) and at concentration of 5 mg/ml (red) and (g) Displacement spectrum of displacement spectral peak of MNPs, at concentration of 10 mg/ml at 2 volt and 3 Hz with different buffered solution MNPs: Phosphate (green) and DI water (red).

**Table I.** Description of experimental setup. (a) Image of the experimental setup. (b) Scheme of the electrical circuit which induces the magnetic field.

Parameter	Type of change	Affect
Coating material	Amine, Dextran and Oleic acid	Oleic acid and Amine coatings mainly alter the frequency of the temporal displacement peak, while Dextran changes the average displacement amplitude as well.
MNPs size	200, 100 and 50 nm	Increase in MNP diameter decreases the frequency of the temporal displacement peak, while at the same time increasing the displacement amplitude
Concentration	10 and 5 mg/ml	Increase in the solution concentration intensify the amplitude of the displacement peak measured.
Voltage	4,3 and 2 volt	By increasing the voltage, the speckle displacement amplified.
Frequency	3,2 and 1 Hz	There is high correlation between MNP displacement peaks and excitation frequencies

Note: Summary table of the manipulated parameters, the type of change and the conclusions deduced from the experiments.

The exact shape, weight and the chemical properties (as surface coating) of the nanoparticle affect the mechanical forces and temporal responsivity they exhibit in a given environment. Those mechanical resonances can be approximated by solving the differential mechanical dynamics equation. The exact frequencies are not required here, as they can be empirically found in the calibration stage. Our aim is to have frequencies which differ from each other in order to allow us to differentiate between the various types of the nanoparticles used as biological markers. Note that there is a shift in the displacement of the MNPs to high frequencies. This phenomenon occurs for low as well as for high applied frequencies, as the magnetic field affects the different coefficients of the differential mechanical dynamics equation.

The illuminated light interacts with the nanoparticles, although they are smaller than half the illumination wavelength. Sub wavelength MNPs causes scattering that result in secondary speckle patterns, then we analyze those patterns. It is impossible to image sub wavelength nanoparticles with resolvable resolution but we only analyze the temporal changes they cause to the scattering.

In this paper a new approach which facilitates speckle imaging by targeted MNPs of various dimensions by applying an external magnetic AC field has been demonstrated. We have shown how capturing a video sequence is used for tracking 2-D speckle pattern movement obtained from MNP displacement under the external magnetic field.

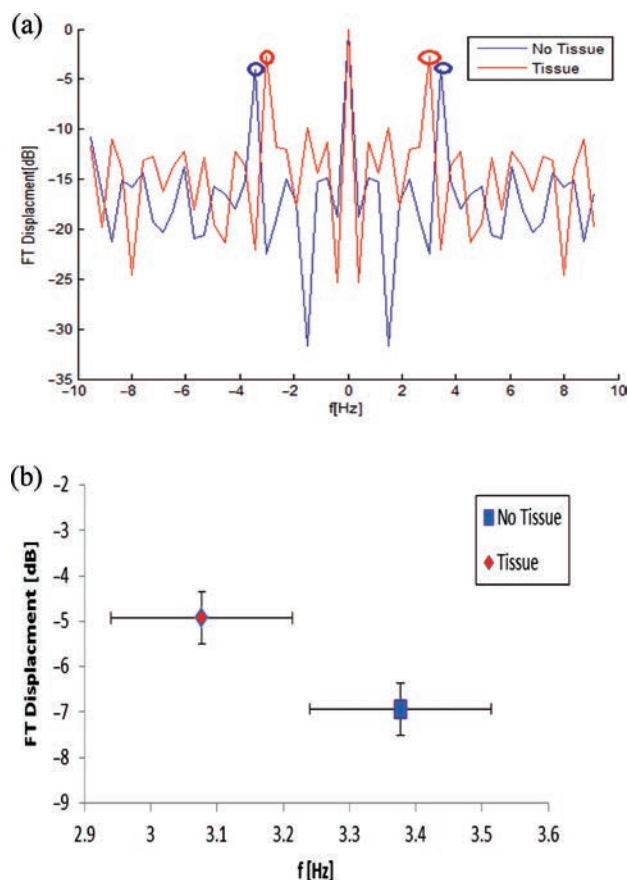


**Fig. 7.** Influence of tissue on MNP displacement spectrum. (a) Displacement spectrum and (b) average amplitude of displacement spectral peak of MNPs for excitation voltage of 4 volt and frequency of 3 Hz w/o tissue screening (blue) and with tissue screening (red).

A correlation was performed between each two consecutive frames of the video sequence for detecting not only the position of the MNPs, but the correlation peak between the two frames as well. The value of the correlation peak defines the relative change in the randomness of the speckle pattern, and corresponds to the axial displacement of the magnetic nano particles.

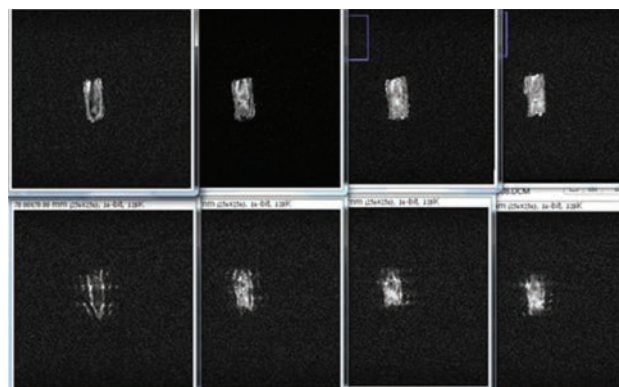


**Fig. 8.** MRI images of atherosclerosis artery without MNPs (top row) and with MNPs (second row).

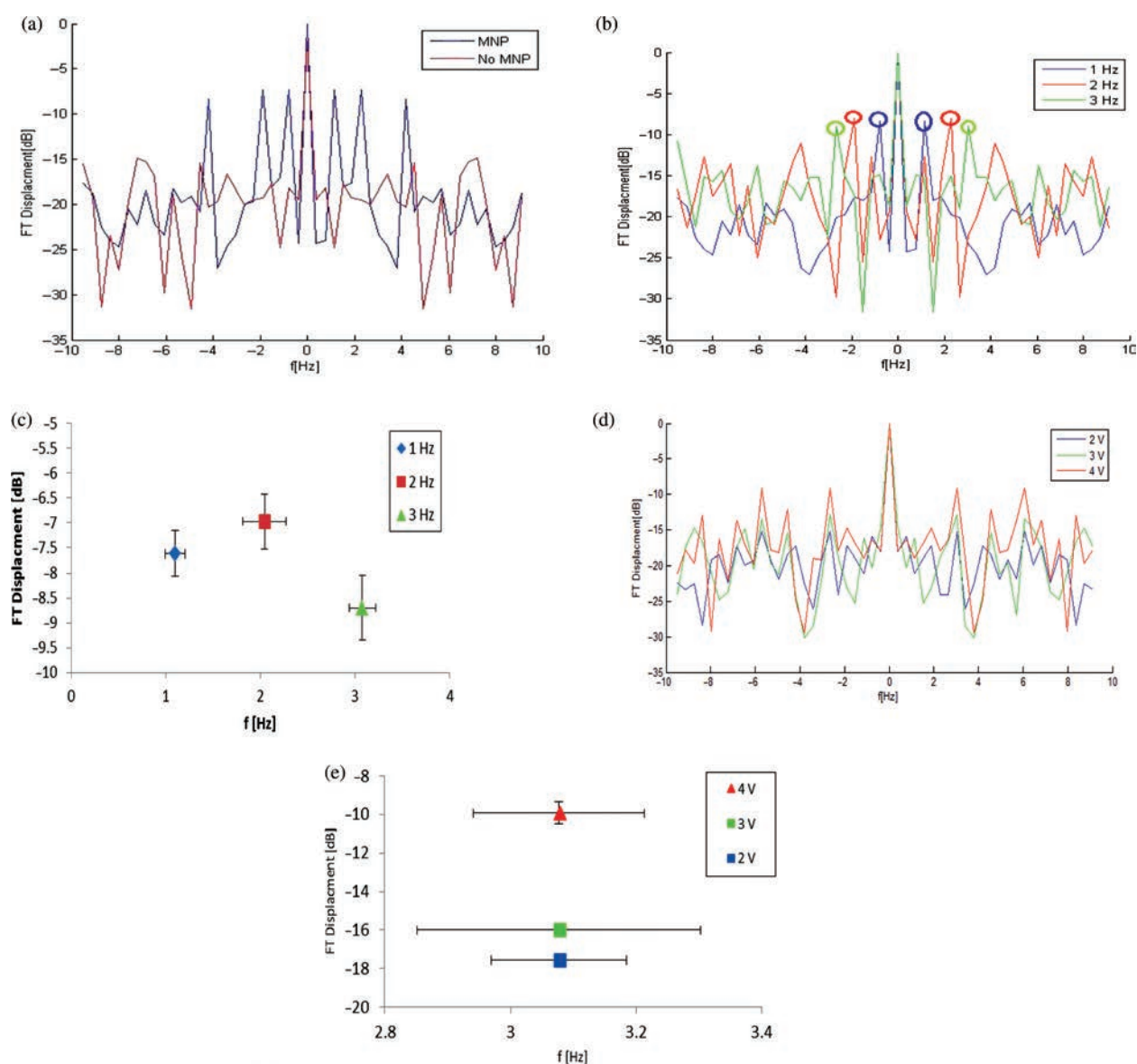


**Fig. 9.** Examining reliability of method for measuring MNPs attached to plaque on a coronary artery *ex vitro*. (a) Displacement spectrum of 200 nm MNPs, attached to plaque on a coronary artery at concentration of 10 mg/ml at 4 volt and 1 Hz (blue) and coronary artery without MNPs (red), (b) Displacement spectrum and (c) average amplitude of displacement spectral peak of 200 nm MNPs, attached to plaque on a coronary artery at concentration of 10 mg/ml at 4 volt and 1 Hz (blue), 2 Hz (red) and 3 Hz (green) and (d) Displacement spectrum and (e) average amplitude of displacement spectral peak of 200 nm MNPs, at concentration of 10 mg/ml at 3 Hz and 4 V (red), 3 V (green) and 2 V (blue).

The result shows a significant difference in the displacement spectrum between different MNPs, due to their different sizes, amount and chemical coating. This indication of the significant difference can lead the speckle imaging by using different coating for different substrates *in-vivo*.

The influence of tissue, which acts as an optically disruptive turbid medium, was examined in *ex-vivo* experiments. A shift in both temporal frequency and amount of displacement as measured by the optical system was found, by taking this into consideration, the method holds great promise for non-invasive speckle imaging. *Ex-vivo* experiments on conjugated MNPs in arterial

plaque provide proof of concept of the method for speckle imaging of atherosclerotic plaques.

CT and MRI imaging are the leading techniques of a whole body imaging. However, due to their disadvantages, such as high cost, complexity etc., there is a quest for other methods. Optical techniques are possible alternatives; however the optical penetration depth limits the use of optical techniques to subcutaneous applications. This work demonstrates a proof of concept for new technique which can be applied for detecting arterial plaques, in a non-invasive way. It has already been demonstrated before that optical technique can be very applicable for biomedical monitoring if they are subcutaneous such as monitoring

tissue thermal modification, monitoring tissue velocity and circulation, imaging techniques observing tissue deformation and tissue motion.<sup>28–31</sup>

The proposed MNP based concept can potentially be developed for dual functionality; not only for detection, but for therapeutic purposes as well, yielding significant clinical applicability. We offer a step towards tissue imaging using targeted MNPs. By mapping a broad platform of speckle displacement for different targeted tissues (such as specific cancer cells or plaque, etc.) and creating a ‘library’ of this data, we vision a molecular imaging that can predict the location or absence of a specific tissue.

## References and Notes

1. K. Rhee and K. S. Park, Binding of atherosclerotic plaque targeting nanoparticles to the activated endothelial cells under static and flow condition, *13th International Conference on Biomedical Engineering IFMBE*, Singapore, CD (2009), Vol. 23, pp. 1785–1787.
2. What Is Atherosclerosis? What Causes Atherosclerosis? <http://www.medicalnewstoday.com/articles/247837.php>.
3. M. Arruebo, R. Fernandez-Pacheco, M. R. Ibarra, and J. S. Magnetic, *Nano Today* 2, 22 (2007).
4. E. Joella and V. Velzen, *J. Cardiology* 50, 245 (2009).
5. G. L. T. Kate, E. J. Sijbrands, and D. Staub, *Current Problems in Cardiology* 35, 556 (2010).
6. K. T. Moe and P. Wong, *Annals of the Academy of Medicine, Singapore* 39, 210 (2010).
7. M. Koneracka and P. Kopčanský, *J. Magn. Magn. Mater.* 252, 409 (2002).
8. O. Veisheh and J. W. M. Zhang, *Advanced Drug Delivery Reviews* 62, 284 (2010).
9. K. Widder, *Proceedings of the Society for Experimental Biology and Medicine* 58, 141 (1978).
10. J. Dobson, *Drug Dev. Res.* 67, 55 (2006).
11. C. Berry and A. Curtis, *J. Phys. D: Appl. Phys.* 36, 198 (2003).
12. T. Jain, J. Richey, and M. Strand, *Biomaterials* 29, 4012 (2008).
13. V. S. Kalambur, B. Han, B. E. Hammer, T. W. Shield, and J. C. Bischof, *Nanotechnology* 16, 1221 (2005).
14. E. Gur and Z. Zalevsky, Iterative single-image digital super-resolution using partial high-resolution data. *World Congress on Engineering* (2007), pp. 5–9.
15. P. Jacquot, *Strain* 44, 57 (2008).
16. Y. Beiderman, A. Amsel, and Y. Tzadka, *Micron* 42, 366 (2010).
17. Z. Zalevsky, *Journal of Electronic Imaging* 18, 1 (2009).
18. M. Ritenberg, E. Beilis, and A. Ilovitsh, *Scientific Reports* 4, 1 (2014).
19. Z. Zalevsky, Y. Beiderman, and I. Margalit, *Opt. Express* 17, 21566 (2009).
20. F. P. Chiang, *Optics and Lasers in Engineering* 47, 274 (2009).
21. M. Qian, J. Liu, M. Yan, Z. Shen, and J. Lu, *Opt. Express* 14, 7559 (2006).
22. Y. Beiderman, I. Horovitz, M. Teicher, J. Garcia, and Z. Zalevsky, *Journal of Biomedical Optics* 15, 1 (2010).
23. M. V. Kristensen, P. Ahrendt, and T. B. Lindballe, *Opt. Express* 20, 1953 (2012).
24. L. Vékás, I. Potencz, D. Bica, and R. Minea, *J. Magn. Magn. Mater.* 65, 223 (1987).
25. F. W. Østerberg, G. Rizzi, and T. Zardán Gómez de la Torre, *Biosens. Bioelectron.* 40, 147 (2013).
26. B. Kuipers, *Rev. Sci. Instrum.* 79, 1 (2008).
27. Q. Pankhurst and J. Connolly, *J. Phys. D: Appl. Phys.* 36, R167 (2003).
28. G. Y. Cho, J. Chan, R. Leano, M. Strudwick, and TH. Marwick, *American Journal of Cardiology* 97, 1661 (2006).
29. A. J. Teske, B. WL. De Boeck, P. G. Melman, G. T. Sieswerda, P. A. Doevendans, and M. J. M. Cramer, *Cardiovasc. Ultrasound* 27 (2007).
30. Y. Tamaki, M. Araie, K. Tomita, A. Tomidokoro, and M. Nagahara, *Surv. Ophthalmol.* 42, S52 (1997).
31. R. L. Maurice and M. Bertrand, *IEEE Trans. Med. Imaging* 18, 593 (1999).

Received: 13 June 2015. Accepted: 3 October 2015.